Rare Metal Materials and Engineering
Volume 54, Issue 4, April 2025
Available online at www.rmme.ac.cn

Science Press

Cite this article as: Wang Bingying, Zhang Keke, Fan Yuchun, et al. Preparation and Brazing Performance of Low-Silver SnAgCu Composite Solder Reinforced by Nickel Coated Al_2O_3[J]. Rare Metal Materials and Engineering, 2025, 54(04): 854-861. DOI: https://doi.org/10.12442/j.issn.1002-185X.20240154.

ARTICLE

Preparation and Brazing Performance of Low-Silver SnAgCu Composite Solder Reinforced by Nickel Coated Al_2O_3

Wang Bingying[1,2], Zhang Keke[1], Fan Yuchun[1], Wu Jinna[1], Guo Limeng[2], Wang Huigai[1], Wang Nannan[1]

[1] Henan University of Science and Technology, Luoyang 471000, China; [2] Luoyang Institute of Science and Technology, Luoyang 471023, China

Abstract: Dopamine polymerization reaction and hydrothermal method were used to prepare nickel coated Al_2O_3 reinforcement phase (Ni/Al_2O_3). Ni/Al_2O_3 reinforced Sn1.0Ag0.5Cu (SAC105) composite solder was prepared using traditional casting method. The result shows that the nickel coating layer is continuous with uneven thickness. The interface between nickel and aluminum oxide exhibits a metallurgical bonding with coherent interface relationship. The strength, toughness and wettability of the SAC105 solder on the substrate are improved, while the conductivity is not decreased significantly. The fracture mode of composites transitions from a mixed toughness-brittleness mode to a purely toughness-dominated mode, characterized by many dimples. The prepared composite brazing material was made into solder paste for copper plate lap joint experiments. The maximum shear strength is achieved when the doping amount was 0.3wt%. The growth index of intermetallic compound at the brazing interface of Ni/Al_2O_3 reinforced SAC105 composite solder is linearly fitted to n=0.39, demonstrating that the growth of intermetallic compound at the interface is a combined effect of grain boundary diffusion and bulk diffusion.

Key words: composite solder; reinforcement phase; polymerization reaction; hydrothermal method; interface

1 Introduction

Due to the harmful effects of lead on the environment, there has been a growing emphasis among scholars on the development of lead-free materials[1–2]. However, SnAgCu solder with high silver content has certain drawbacks, such as poor drop impact performance and high cost[3–5]. Therefore, the study of low-silver alloy solder has become a prominent research direction. Previous studies have found that low silver content can lead to some challenges, such as decreased spreading area and low tensile strength[6–7]. Therefore, the development of a low-silver solder with superior comprehensive performance has become a focus for scholars.

Currently, there are two common methods to improve composite solder: one involves adding alloy elements to the solder for melting, the other is adding second phase to the base solder[8–10]. In recent years, the doping of inert particles has become a research hotspot in the realm of second phase modifications[11–13]. Nano alumina has advantages of light-weight and cost-effectiveness, making it well-suited for high-density packaging technology[14–15]. However, the interface adhesion between nano alumina and the solder alloy matrix is weak, resulting in poor wettability and toughness of the composite solder[16–19]. Nickel particles have advantages such as larger specific surface area, uniform dispersion of active components, and resistance to sintering, which can effectively prevent agglomeration. Studies have shown that the addition of an appropriate amount of nickel can refine the microstructure and improve service performance of solder alloys[20].

Received date: April 17, 2024
Foundation item: National Natural Science Foundation of China (U1604132); Central Plains Talents Program-Fund of Central Plains Leading Talents (ZYYCYU002130); Key Technology Research and Development Program of Henan Province (222102230114); Major Scientific Research Foundation of Higher Education of Henan Province (23B430003)
Corresponding author: Zhang Keke, Ph. D., Professor, Henan University of Science and Technology, Luoyang 471000, P. R. China, E-mail: zhkeke@haust.edu.cn

Due to poor wettability of ceramics and metals, it is difficult to connect them together. Unlike metal bonds, ceramics are composed of covalent bonds[21]. Therefore, the bonding strength of the ceramic/metal interface is poor. Dopamine polymerization reaction was adopted. Firstly, amorphous carbon film was applied as a transition layer on the surface of alumina, as it is more capable of adsorbing nickel ions. Then, nickel nitrate was used as the precursor by hydrothermal method, and after the reaction was completed, the amorphous carbon film was burned off and the nickel coated layer was left behind by calcination in an air atmosphere.

2 Experiment

The Sn1.0Ag0.5Cu (SAC105) power with a particle size of 50 μm, provided by Changsha Tianjiu Company, was used in the experiment. Dopamine hydrochloride and trimethylaminomethane were purchased from McLean Technology Co., Ltd (China). Nickel nitrate hexahydrate (AR) and nano-Al_2O_3 particles were purchased from PanTian Co., Ltd (Shanghai, China).

The reinforcing phase of the composite solder was nickel coated Al_2O_3, and the reaction principle of coating is shown in Fig. 1. The specific description is as follows: a specific quantity of Al_2O_3 nanoparticles and dopamine were dispersed into a tri(hydroxymethyl)aminomethane buffer solution. Dopamine underwent spontaneous oxidation, forming polydopamine coated Al_2O_3 particles. After heat treatment in an argon atmosphere, polydopamine was converted into nitrogen-containing carbon and coated on the surface of Al_2O_3. Then, the nickel salt was heated and decomposed by hydrothermal method, and the carbon coated in the first step was burned off in an air atmosphere. Finally, the nickel layer was coated on the surface of Al_2O_3.

The equations for hydrothermal reaction are as follows.

$$Ni(NO_3)_2 \rightleftharpoons Ni^{2+} + 2NO_3^- \quad (1)$$

$$Ni^{2+} + 2OH^- \rightarrow Ni(OH)_2 \quad (2)$$

$$Ni(OH)_2 \triangleq NiO + H_2O \quad (3)$$

$$2NiO + C \rightarrow 2Ni + CO_2 \uparrow \quad (4)$$

The preparation of brazed joints in this experiment was carried out using copper plate overlap method. Composite solder paste was used to fill the gap between two copper plates. SAC105 alloy powder possessed size of 25 – 40 μm. Nano Ni/Al_2O_3 particles with average size of 200 nm were used to synthesize the composite solder SAC105-x(Ni/Al_2O_3) (x=0.0, 0.1, 0.3, 0.5, wt%). The specific process is as follows. Ni/Al_2O_3 particles and paste were weighed using an electronic balance, manually mixed, and quickly stirred for 30 min. Afterwards, SAC105 alloy powder was added to the mixture and manually stirred for at least 30 min to ensure that the composite solder achieved desired viscosity and that Ni/Al_2O_3 particles were uniformly dispersed in the composite solder[22]. The specific size of copper plate overlap is shown in Fig.2.

The morphology of the prepared Ni-Al_2O_3 was observed by scanning electron microscope (SEM) and transmission electron microscope (TEM). The phase structure was analyzed by X-ray diffractometer (XRD) with Cu Kα radiation at a scan rate of 0.4 nm/min and accelerating voltage of 40 kV within scan range of 20° – 90°. The composition of Ni-Al_2O_3 was measured by energy dispersive spectroscope (EDS). The polished specimens were etched in a mixture of methanol and hydrochloric acid (92vol% methanol and 8vol% hydrochloric acid) for 20 s. X-ray photoelectron spectroscopy (XPS) is a common surface analysis method, which was used to analyze the composition, chemical state, and molecular structure of sample surface.

3 Results and Discussion

3.1 Composition and morphology analysis of nickel coated Al_2O_3

Fig.3 shows XRD patterns of Al_2O_3 before and after nickel coating. Sharp characteristic peaks are displayed at 25.6°, 35.2°, 37.8°, 43.4°, 52.6°, 57.5° and 66.5°, corresponding to (110), (211), (1$\bar{1}$0), (210), (220), (321), (310) and (12$\bar{1}$) planes of the Al_2O_3 crystal structure, respectively. The peak value is consistent with the standard card (PDF # 74-1081). The peaks of nickel appear at 44.5° and 51.8°, corresponding to the (111)

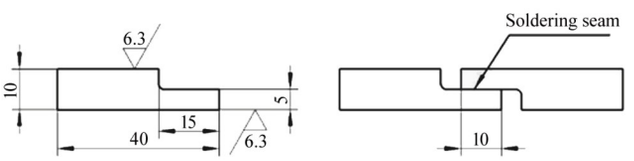

Fig.2 Schematic diagram of copper plate overlap during brazing process

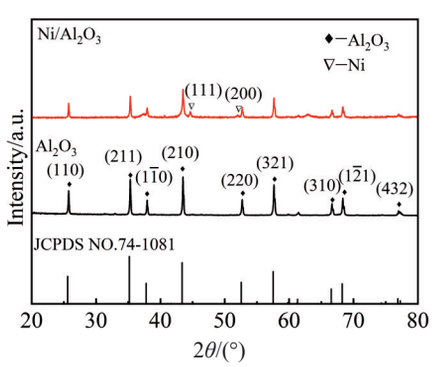

Fig.3 XRD patterns of Al_2O_3 before and after nickel coating

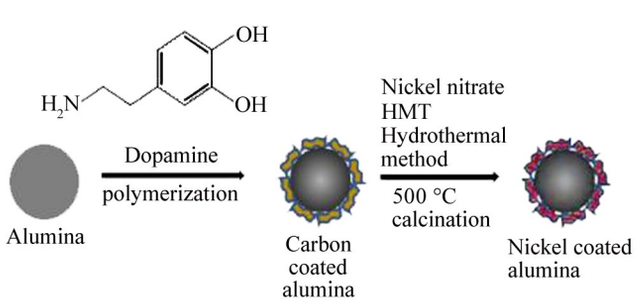

Fig.1 Principle diagram of nickel coated Al_2O_3 reaction

and (200) crystal planes, respectively.

Fig.4 shows TEM results of nickel coated Al_2O_3. In Fig.4e, the distribution of element Ni is uniform and continuous. In Fig.4f, the distribution of element C is very scattered, without obvious bright areas, indicating that amorphous carbon has been decomposed in the early stage. Fig.4g shows the high-resolution TEM image of the interfaces. The Ni/Al_2O_3 interface can be assigned to Ni (111)/Al_2O_3 (110) interface, where d_{Ni}=0.245 nm and $d_{Al_2O_3}$=0.215 nm. Eq.(5) represents the mismatch (ε) between the two interfaces.

$$\varepsilon=(d\alpha-d\beta)/d\alpha \quad (5)$$

where $d\alpha$ is the interplanar spacing of interface α (nm), and $d\beta$ is the interplanar spacing of interface β (nm). According to the formula, ε =0.13 is calculated. According to Ref. [23], if ε ranges from 0.05 to 0.25, the interface shows a semi-coherent relationship. This means that the interface is metallurgically bonded, so the coating will not fall off.

Fig.5a shows total characteristic spectra of alumina before and after nickel modification, in which more characteristic peaks of nickel are present in the Ni/Al_2O_3. Due to nickel coating, the peak content of aluminum on the surface is significantly reduced. Fig.5b shows the spectra of aluminum

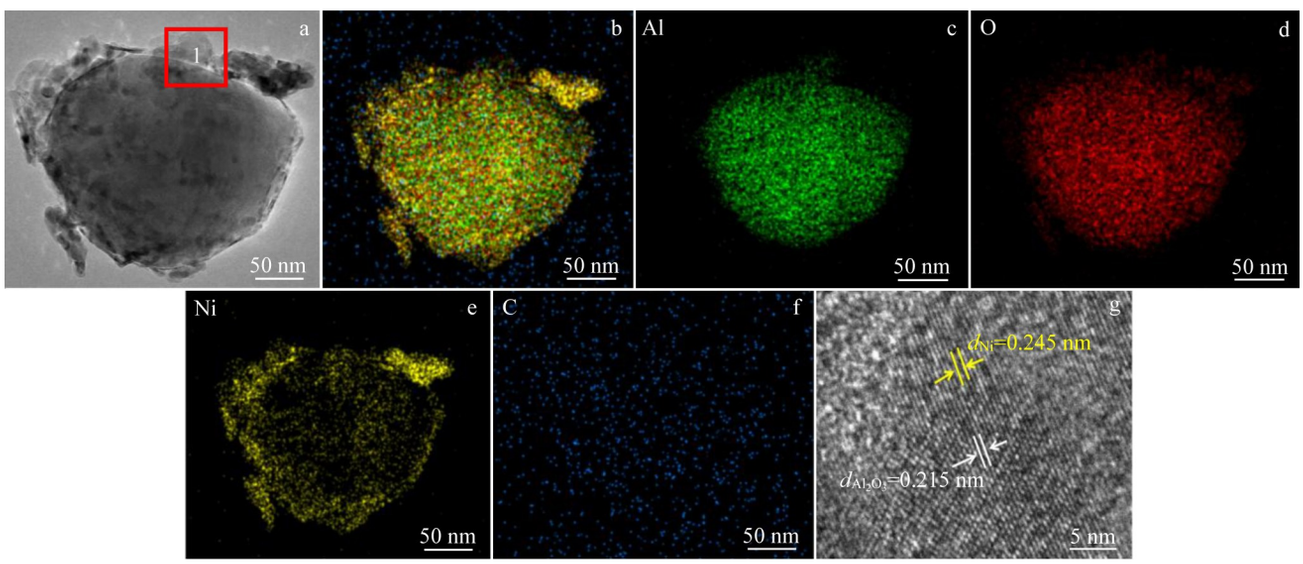

Fig.4 TEM image (a) and EDS mappings (b–f) of Ni/Al_2O_3; high-resolution TEM image of region 1 in Fig.1a (g)

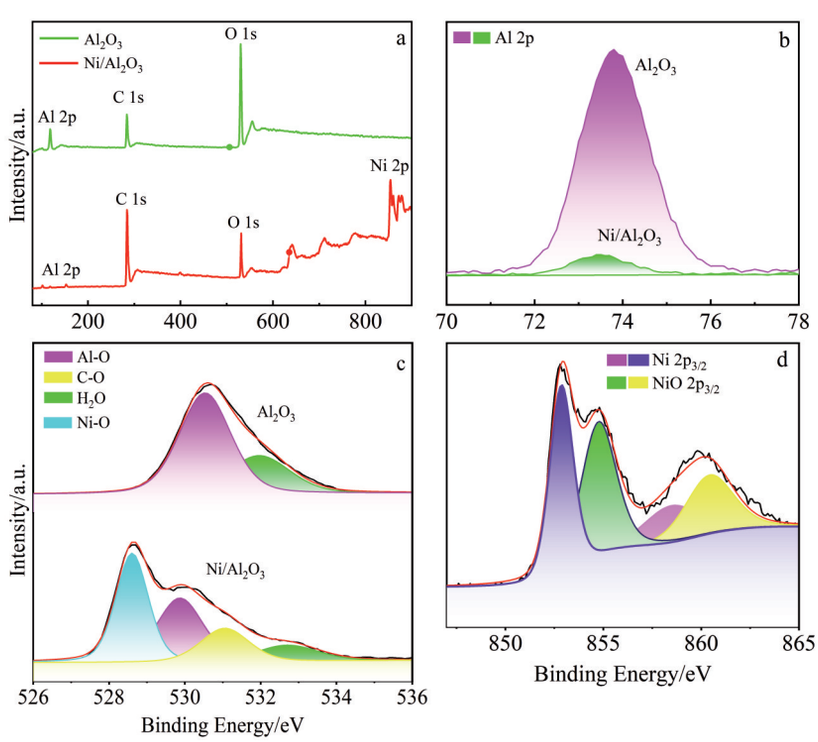

Fig.5 XPS spectra of Al_2O_3 and Ni/Al_2O_3: (a) total spectra, (b) Al 2p, (c) O 1s, and (d) Ni 2p

before and after nickel modification. It can be seen that the peak appears around 74 eV, which is determined to be Al 2p[24]. The decrease in peak intensity is consistent with the tendency in total spectra, which is due to the reduction of surface aluminum elements caused by nickel coating. Aluminum oxide is not participated[25]. Fig. 5c shows the O 1s peak before and after nickel modification. According to the NIST XPS database, C-O and Ni-O peaks at 531.2 and 528.3 eV increase for Ni/Al_2O_3 sample, respectively. Fig. 5d shows the Ni 1s peak in the Ni/Al_2O_3 sample. Peaks of Ni $2p_{3/2}$, NiO $2p_{3/2}$, Ni $2p_{3/2}$ (sat) and NiO $2p_{3/2}$ (sat) are detected at 852.9, 854.8, 858.6 and 860.5 eV, respectively, indicating the presence of nickel in the sample, which is consistent with XRD analysis results.

3.2 Microstructure and properties of composite solder

Fig. 6 shows the microstructures of the composite solder. In Fig. 6a, the microstructure of SAC105 raw solder mainly includes β-Sn and eutectic structure. The gray block area is β-Sn, the eutectic structure is a white area, which is mainly concentrated on the grain boundary structure line. With the increase in addition content of Ni/Al_2O_3 particles, the β-Sn area gradually decreases, and the proportion of eutectic structure gradually increases. The possible reason may be that most of the Ni/Al_2O_3 particles adhere to the surface of the solder alloy powder, leading to an increase in the surface diffusion resistance of atoms during the sintering process. Since the merging and growth of β-Sn grains are restricted, the average size of β-Sn grains decreases and the proportion of eutectic structure increases. When the content of Ni/Al_2O_3 particles exceeds 0.5wt%, agglomeration occurs, reducing its uniformity in the base solder. This further weakens the grain refinement effect and leads to coarsening of the eutectic structure[26].

Fig. 7 shows the trend of wetting area and electrical conductivity of composite solder with different mass fractions of Ni/Al_2O_3 reinforcement phases. Wettability represents the diffusion degree of fluid on solid surfaces[27]. As the content of Ni/Al_2O_3 in the solder matrix increases, the wetting area firstly increases and then decreases. The reason for this change may be explained as follows. During the wetting process, Ni/Al_2O_3 particles fill the interface between the composite solder and the copper substrate through capillary action[28]. When Ni/Al_2O_3 particles are added, the agglomeration of Ni/Al_2O_3 in the solder matrix increases, which reduces the gap between the intermetallic compound (IMC) layer at interface, leading to thermal expansion between the solder matrix and reinforcement phase, and causing oxidation of the composite solder, thereby reducing its fluidity and wettability[29–31].

As the content of Ni/Al_2O_3 increases, the electrical conductivity of the composite solder slightly decreases. This change can be explained by Mattison's law. The electrical resistivity of metal materials can be expressed as: $\rho(T)=\rho_e(T)+\rho_0$, where $\rho_e(T)$ is a temperature dependent resistivity and it is called the basic resistance; ρ_0 is related to impurity concentration, point defects and and it is called solute (impurity) resistance of metals[32]. Introducing Ni/Al_2O_3 into the SAC105 solder matrix results in defects such as vacancies, dislocations and interfaces, which hinder electron migration and increase resistance. However, due to the small quantity of reinforcing phase added, the decrease in conductivity is not significant.

Fig. 8 illustrates the mechanical properties of SAC105 solder reinforced with different mass fractions of Ni/Al_2O_3. With the increase in the doping amount of the reinforcement phase, both the tensile strength and elongation show the same trend of first increasing and then decreasing. When the doping content reaches 0.3wt%, the tensile strength and elongation of the modified solder reach the maximum, which are 16% and

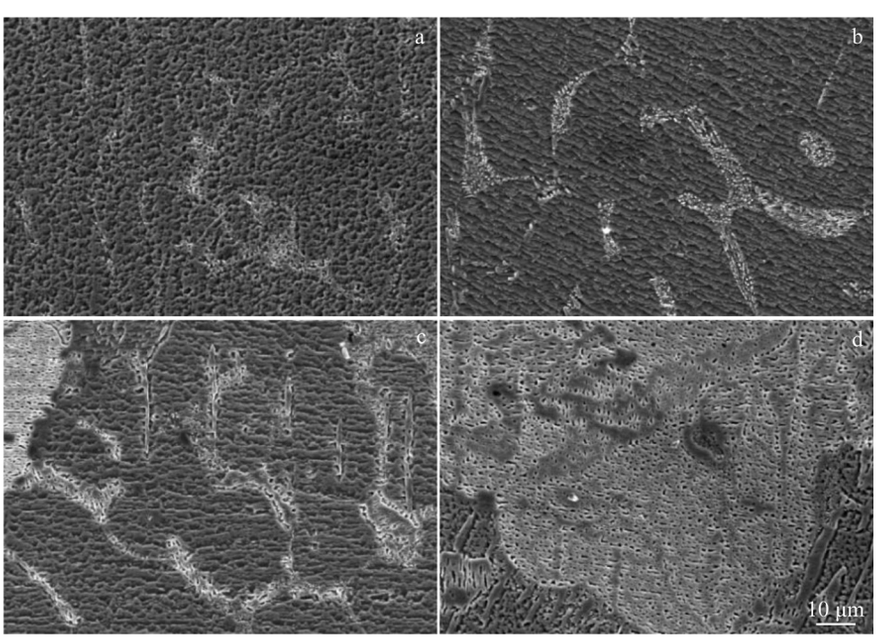

Fig.6 Microstructures of SAC105-x(Ni/Al_2O_3) composite solder: (a) raw solder, (b) x=0.1wt%, (c) x=0.3wt%, and (d) x=0.5wt%

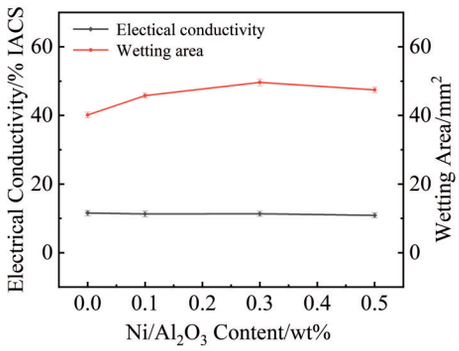

Fig.7 Performance of SAC105 solder reinforced with different contents of Ni/Al_2O_3

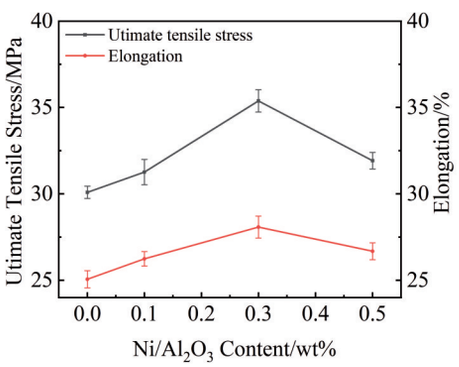

Fig.8 Mechanical properties of SAC105 solder reinforced with different contents of Ni/Al_2O_3

8% higher than those of the original solder, respectively. Afterwards, as the mass fraction of the enhancement phase continues to increase to 0.5wt% , the tensile strength and elongation of the brazing material decrease to 32 MPa and 26%, respectively. The reason for the decrease in strength and elongation may be excessive agglomeration of reinforcement phases. In summary, when 0.3wt% Ni/Al_2O_3 is added, the tensile strength (35.3 MPa) and elongation (28.1%) of the composite solder reach their maximum values, which is better than other similar nanomaterials previously reported to enhance SAC105 composite solder[33]. Meanwhile, compared to commercial Sn3.0Ag0.5Cu[34–35], the ultimate tensile strength results are basically the same, with higher elongation than that of commercial Sn3.0Ag0.5Cu. These results indicate that this new type of lead-free solder can obtain materials with high strength and ductility.

3.3 Shear strength and interface IMC of brazed joints

Fig. 9 illustrates the shear strength of solder joints brazed with different contents of Ni/Al_2O_3. As the content of Ni/Al_2O_3 increases to 0.1wt%, 0.3wt% and 0.5wt%, the shear strength of the composite alloy increases by 6%, 16% and 10%, respectively, compared with those of the original SAC105 solder.

Fig. 10 illustrates the fracture morphologies of SAC105 solder with different reinforcement phase contents. The fracture morphology of the raw solder is shown in Fig. 10a.

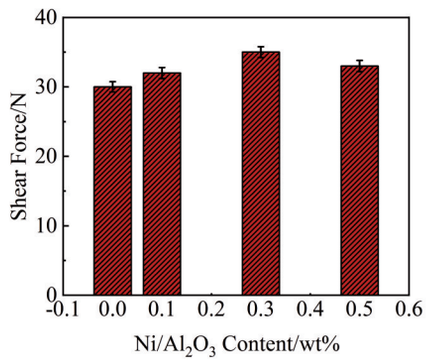

Fig.9 Shear strength of solder joint with SAC105-x(Ni/Al_2O_3) solders (x=0.0, 0.1wt%, 0.3wt%, 0.5wt%)

The fracture surface is mainly composed of ductile dimples and brittle cleavage planes, indicating that its fracture mode is ductile brittle fracture. With the increase in Ni/Al_2O_3 content, the number and depth of ductile dimples increase, indicating a greater degree of plastic deformation. In addition, the number of cleavage planes on the fracture surface decreases. As shown in Fig. 10c, when the doping content reaches 0.3wt% , the number of dimples is the highest and the plasticity is the best, which is consistent with the previous change in elongation.

Based on the above analysis, it can be concluded that the optimal addition amount is 0.3wt%. At different brazing time, brazing experiments were conducted on composite solder with 0.3wt% enhancement phases, and the diffusion mechanism of IMC formation in brazed joints was studied.

Fig. 11 shows the microstructures of the interface IMC of the SAC105-0.3wt% Ni/Al_2O_3 composite brazing joint. It can be seen that when the brazing time is 180 s, the interface IMC is scallop-shaped, with a relatively uniform particle size distribution and an average thickness of about 3.16 μm. When the brazing time is 240 s, the overall interface IMC still presents a scallop-like shape, with uneven particle sizes and an average thickness of about 3.27 μm. When the brazing time is 300 s, the interface IMC shows a partially serrated shape, with uneven particle sizes and an average thickness of 3.34 μm. When the brazing time is 360 s, the interface IMC transforms into a coarse serrated shape, with an average thickness of 4.32 μm.

During the brazing process, the growth of the interface IMC layer is a complex process. When Cu atoms and Sn atoms react with each other to form Cu_6Sn_5 compounds, the further growth of interface IMC is mainly controlled by diffusion, which includes two stages: grain boundary diffusion and bulk diffusion. The relationship between the thickness of IMC at the composite brazing interface and brazing time is expressed as Eq.(6):

$$x=kt^n \quad (6)$$

where x is the average thickness of interface IMC with different brazing durations; k is a constant; t is the brazing time; n is the time index of interface IMC growth.

Take the logarithm on both sides of Eq.(6) to obtain Eq.(7)

$$\ln x=\ln k+n\ln t \quad (7)$$

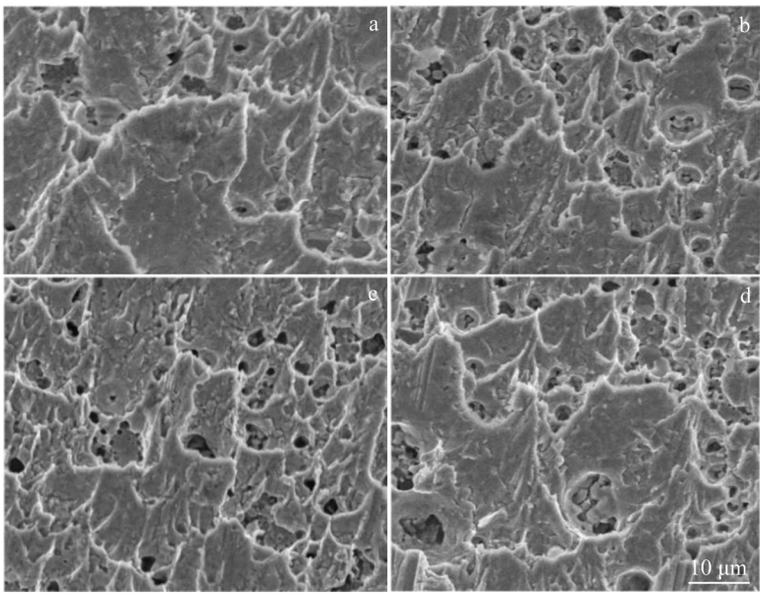

Fig.10 Microstructures of SAC105-x(Ni/Al_2O_3): (a) raw solder; (b) x=0.1wt%; (c) x=0.3wt%; (d) x=0.5wt%

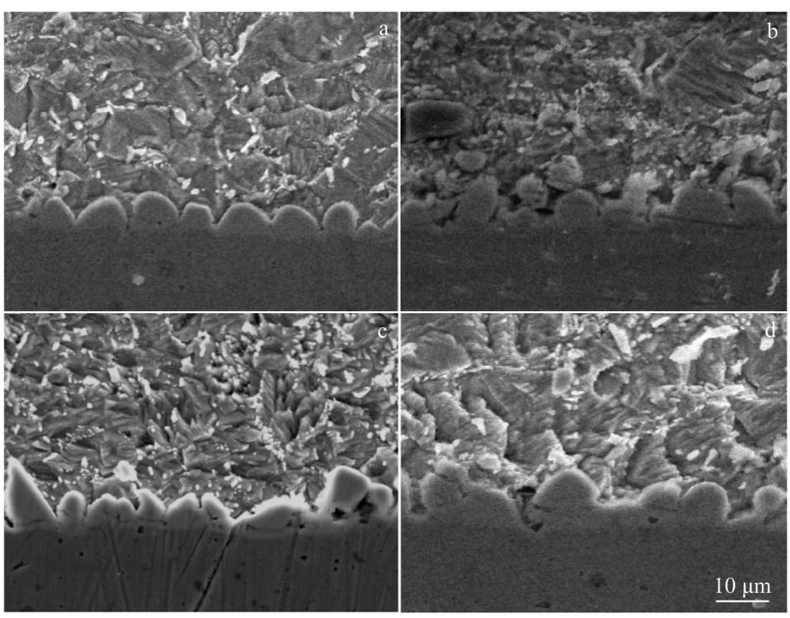

Fig.11 Morphologies of IMC at the joint interface of SAC105-0.3wt% Ni/Al_2O_3 with different brazing durations: (a) 180 s, (b) 240 s, (c) 300 s, and (d) 360 s

Using ln$t$ as the horizontal axis and ln$x$ as the vertical axis, a linear function can be obtained by fitting, and the slope of the function interface is the growth index n of IMC. According to the fitting, the growth index n of IMC at the brazing interface of Ni/Al_2O_3 reinforced SAC105 composite solder is 0.39. According to Ref.[36], when the interface IMC growth is controlled by grain boundary diffusion, the growth time index n is 0.33; when the growth of interface IMC is controlled by bulk diffusion, the growth time index n is 0.50. Therefore, the growth of interface IMC during the brazing process is the result of the combined effect of grain boundary diffusion and bulk diffusion.

4 Conclusions

1) Nickel coated alumina reinforcement phase can be prepared by dopamine polymerization reaction and hydrothermal method. In the coating process, the nickel layer formed is uniform and continuous.

2) When the adding amount of Ni/Al_2O_3 varies to 0.1wt%, 0.3wt% and 0.5wt%, the conductivity of the brazing alloy material slightly decreases. The overall wettability of composite materials is improved compared with that of the matrix materials, and the wettability is the best when the adding amount is 0.3wt%.

3) With the increase in adding amount of Ni/Al_2O_3, the overall tensile strength and elongation of the composite material are improved compared to those of the matrix. When the Ni/Al_2O_3 content reaches 0.3wt%, the tensile strength and elongation reach the maximum, and the toughness of the fracture also reaches the maximum.

4) The growth index of IMC at the brazing interface of SAC105-0.3wt% Ni/Al_2O_3 is linearly fitted to n=0.39, indicating that the growth of IMC at the interface is the result of the combined effect of grain boundary diffusion and bulk diffusion.

References

1 Huo F B, Zhi J, Han D L *et al. Materials & Design*[J], 2021, 210: 110038

2 Sharma A, Baek B G, Jung J Pu *et al. Materials & Design*[J], 2015, 87: 370

3 Xu S Y, Habib A H, Pickel A D *et al. Progress in Materials Science*[J], 2015, 67: 95

4 Kotadia H R, Howes P D, Mannan S H. *Microelectronics Reliability*[J], 2014, 12(6–7): 1253

5 Lin Y L, Wang W. *Microelectronics Reliability*[J], 2014, 8: 56

6 Wu J, Xue S B, Wang J W *et al. Journal of Materials Science*[J], 2016, 27: 12729

7 Ma H T, Suhling J C *et al. Journal of Materials Science*[J], 2009, 44: 1141

8 Zhang M, Zhang K K, Huo F *et al*. *Materials & Design*[J], 2019, 12: 289

9 Li Z H, Tang Y, Guo Q W *et al. Journal of Alloys and Compounds*[J], 2019, 818: 152893

10 Jung D H, Sharma A, Jung J P *et al. Journal of Alloys and Compounds*[J], 2018, 743: 300

11 Mohd Nasir S S, Yahaya M Z, Erer A M *et al. Ceramics International*[J], 2019, 45(15): 18563

12 Li Z H, Tang Y, Guo Q W *et al. Journal of Alloys and Compounds*[J], 2019, 789: 150

13 Wang B Y, Wu Y J, Wu W *et al. Journal of Materials Science*[J], 2022, 57: 17491

14 Wu J, Xue S B, Wang J W *et al. Journal of Materials Science: Materials in Electronic*s[J], 2018, 29: 7372

15 Shalaby R M, Elzanaty H *et al. Journal of Materials Science: Materials in Electronics*[J], 2020, 31: 5907

16 Yakymovych A, Plevachuk Y, Svec P *et al. Journal of Materials Science: Materials in Electronics*[J], 2016, 45: 6143

17 Tikale S, Prabhu K N. *Materials Science and Engineering A*[J], 2020, 787: 139439

18 Tikale S, Prabhu K N. *Transactions of the Indian Institute of Metals*[J], 2018, 71: 2855

19 Tsao L C, Chang S Y, Lee C I *et al. Materials & Design*[J], 2010, 31(10): 4831

20 Wang Y L, Wang G X, Song K X *et al. Materials & Design*[J], 2017, 119: 219

21 Tikale S, Prabhu K N. *Journal of Materials Science: Materials in Electronics*[J], 2021, 32: 2865

22 Wang J H , Xue S B, Lv Z P *et al. Progress in Materials Science*[J], 2019, 33: 13

23 Yang J, Xu L, Xu K *et al. Steel Research International*[J], 2015, 5: 619

24 He J Q, Sun J L, Choi J *et al. Friction*[J], 2023, 11: 441

25 Zhang Cunliang. *Modification of NASICON Type Electrode Material Lithium Vanadium Phosphate Research on Preparation and Lithium Storage Properties*[D]. Nanjing: Nanjing University of Aeronautics and Astronautics, 2016 (in Chinese)

26 Zhang L, Zhang J G, Liu F G *et al. Rare Metal Materials and Engineering*[J], 2013, 42: 1897

27 Liu G P, Li Y L, Long W F *et al*. *Journal of Alloys and Compounds*[J], 2019, 802: 345

28 Landry K, Eustathopoulo N *et al. Acta Materialia*[J], 1996, 44(10): 3923

29 Wang Y L, Fang Z H, Ma N *et al. Journal of Materials Science: Materials in Electronics*[J], 2017, 28: 94

30 Lai Y Q, Hu X W, Jiang X X *et al. Journal of Materials Engineering and Performance*[J], 2018, 27: 6564

31 Yang Z B, Zhou W, Wu P *et al. Journal of Materials Engineering & Performance*[J], 2014, 590: 295

32 Wang H G, Zhang K K, Zhang M *et al. Journal of Alloys & Compounds*[J], 2019, 781: 761

33 El-Daly A A, Fawzy A. *Materials Science and Engineering A*[J], 2013,578:62

34 Han Y D, Nai S M L, Jing H Y *et al*. *Journal of Materials Science: Materials in Electronics*[J], 2011, 22: 315

35 Gain A K, Chan Y C. *Microelectronics Reliability*[J], 2014, 54: 945

36 Yu D Q, Wang L. *Journal of Alloys and Compounds*[J], 2008, 458(1–2): 542

镍涂层Al_2O_3增强低银SnAgCu复合钎料的制备及钎焊性能

王冰莹[1,2]，张柯柯[1]，范玉春[1]，吴金娜[1]，郭李梦[2]，王悔改[1]，王楠楠[1]
(1. 河南科技大学，河南 洛阳 471000)
(2. 洛阳理工学院，河南 洛阳 471023)

摘　要：采用多巴胺聚合反应和水热法制备了镍包覆氧化铝增强相（Ni/Al_2O_3）；使用传统铸造方法制备Ni/Al_2O_3增强Sn1.0Ag0.5Cu（SAC105）复合钎料。结果表明，镍涂层是连续的，但厚度不均匀。镍与氧化铝之间的界面是冶金结合的半相干界面关系；SAC105焊料与基体的强度、韧性和润湿性得到了改善，而导电性并没有显著降低。复合材料合金的断裂模式从韧脆性混合断裂转变为纯韧性断裂。将制备的复合钎焊材料制成焊膏进行铜板搭接实验。当掺杂量为0.3wt%时，达到最大剪切强度。复合钎料钎焊接头界面处金属间化合物的生长指数线性拟合为n=0.39，表明钎焊接头界面处金属间化合物生长为晶界扩散和体扩散共同作用的结果。

关键词：复合钎料；增强相；聚合反应；水热法；界面

作者简介：王冰莹，女，1984年生，博士，河南科技大学，河南 洛阳 471000，E-mail：353315856@qq.com